Available online at www.sciencedirect.com
SCIENCE DIRECT®
Thin Solid Films 496 (2006) 160 – 168
thin solid films
www.elsevier.com/locate/tsf

Charge carrier and spin doping in ZnO thin films

D.P. Norton [a,*], M. Ivill [a], Y. Li [a], Y.W. Kwon [a], J.M. Erie [a], H.S. Kim [a], K. Ip [a], S.J. Pearton [a], Y.W. Heo [b], S. Kim [c], B.S. Kang [c], F. Ren [c], A.F. Hebard [d], J. Kelly [d]

[a] Department of Materials Science and Engineering, University of Florida, Gainesville, FL 32611, United States
[b] Kyungpook National University, Department of Inorganic Materials Engineering, Daegu, 702-701, Republic of Korea
[c] Department of Chemical Engineering, University of Florida, Gainesville, FL 32611, United States
[d] Department of Physics, University of Florida, Gainesville, FL 32611, United States

Available online 30 September 2005

Abstract

Recent efforts on doping ZnO films for charge and spin functionality are reviewed, focusing on chemical doping for charge and spin device formation. Discussion includes the behavior of phosphorus as an acceptor and magnetism in transition metal-doped ZnO. Evidence for p-type behavior in phosphorus-doped (Zn,Mg)O grown by pulsed laser deposition is presented. The magnetic properties of ZnO co-doped with Mn and Sn are also discussed.

Keywords: Zinc oxide; Semiconductors; Magnetic properties and measurements

1. Introduction

ZnO is an attractive semiconductor for solid state blue to UV optoelectronics, including laser development. Transparency to visible light provides opportunities to develop transparent electronics, UV optoelectronics, and integrated sensors, all from the same material system. ZnO is a direct band gap semiconductor with E_g=3.2 eV. Doping with certain transition metal dopants is predicted to yield ferromagnetism. The room temperature electron Hall mobility in ZnO single crystals is on the order of 200 cm^2/V s [1]. ZnO normally forms in the hexagonal (wurtzite) crystal structure shown in Fig. 1, with a=3.25 Å and c=5.12 Å. Each Zn atom is tetrahedrally coordinated to four O atoms, where the Zn d-electrons hybridize with the O p-electrons. Layers occupied by zinc atoms alternate with layers occupied by oxygen atoms. Electron doping in nominally undoped ZnO has been attributed to Zn interstitials, oxygen vacancies, or hydrogen [2–7]. The intrinsic defect levels that lead to n-type doping lie approximately 0.05 eV below the conduction band. High electron carrier density can also be realized via group III substitutional doping. The semiconducting properties of ZnO compare favorably to those of the GaN system, as is seen in Fig. 2. The band gap of ZnO can be tuned via divalent substitution on the cation site. Cd substitution leads to a reduction in the band gap to ~3.0 eV [8]. Substituting Mg on the Zn site in epitaxial films can increase the band gap to approximately 4.0 eV while still maintaining the wurtzite structure. The latter represents a metastable compound that is stabilized via epitaxial film growth. Epitaxial wurtzite $Zn_{1-x}Mg_xO$ thin films have been realized with x as large as 0.35 [9,10]. The (Zn,Mg)O alloy system is attractive for UV photonics needed in the next generation optical memory, integrated optics with sub-micron feature size, visible–blind UV detectors, and spectroscopic-based detection of biological and chemical agents [11].

2. P-type doping in ZnO

A significant challenge to the widespread exploitation of ZnO-related materials in electronic and photonic applications is the difficulty in achieving p-type material. ZnO displays significant resistance to the formation of shallow acceptor levels. Difficulty in achieving bipolar (n- and p-types) doping in a wide band gap material is not unusual. ZnSe and GaN can be easily doped n-type, while p-type doping is difficult. In contrast, ZnTe is difficult to dope n-type, while p-type doping is easily achieved. There have been several explanations put forward in

* Corresponding author. Tel.: +1 352 846 0525; fax: +1 352 846 1182.
E-mail address: dnort@mse.ufl.edu (D.P. Norton).

0040-6090/$ - see front matter © 2005 Elsevier B.V. All rights reserved.
doi:10.1016/j.tsf.2005.08.246

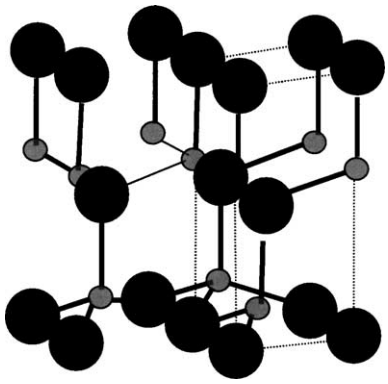

Fig. 1. Wurtzite crystal structure.

explaining doping difficulties in wide gap semiconductors [12]. First, there can be compensation by native point defects or dopant atoms that locate on interstitial sites. The defect compensates for the substitutional impurity level through the formation of a deep level trap. In some cases, strong lattice relaxations drive the dopant energy level deep within the gap. One may also have a low solubility for the chosen dopant limiting the accessible extrinsic carrier density [13]. In ZnO, most candidate p-type dopants introduce deep acceptor levels. Copper doping introduces an acceptor level with an energy of ~0.17 eV below the conduction band [14]. Silver has also been investigated; it behaves as an acceptor with a deep level ~0.23 eV below the conduction band [15]. Lithium introduces a deep acceptor, and induces ferroelectric behavior [16,17].

The most promising dopants for p-type material are the group V elements, although theory suggests some difficulty in achieving shallow acceptor states [18]. While ab initio electronic band structure calculations for ZnO based on the local density approximation indicate that the Madelung energy decreases with group III cation substitution for n-type doping [19], the Madelung energy increases with group V anion substitution indicating localization of these acceptor states. Nevertheless, there have been reports suggesting acceptor doping with group V substitution. Photoinduced paramagnetic resonance studies of N-doped ZnO crystals indicate the presence of an acceptor state due to nitrogen substitution [20]. Minegishi et al. reported the growth of p-type ZnO by the simultaneous addition of NH_3 in hydrogen carrier gas with excess Zn [21]. The resistivity of these films was high with $\rho \sim 100\ \Omega$ cm, suggesting that the acceptor level is relatively deep with a subsequent low mobile hole concentration. P-type ZnO has also been reported for films grown by PLD, in which a N_2O plasma is used for doping [22]. Efforts by Rouleau et al. [23] have addressed nitrogen doping in epitaxial ZnO films in which a RF plasma source was used to crack N_2 in conjunction with Zn evaporation during pulsed laser deposition from a ZnO target. Secondary ion mass spectrometry data for N-doped ZnO films clearly shows that the films contain nitrogen. However, no definitive p-type behavior was observed, suggesting that compensating complexes are incorporated in the growing film. Similar results have been reported by others [24]. The lack of p-type behavior in nitrogen-doped ZnO has been addressed theoretically within the context of N–N complex formation [25]. In particular, it appears that the formation of N–N related complexes introduce compensating centers. Isolated substitutional N is assumed to be required to realize an acceptor state. As such, the use of source species that contain only one nitrogen atom per entity (NO, N, NO_2) should be more amenable to acceptor state formation due to the large dissociation energy of N_2 (9.9 eV). Recently, promising results were reported on the synthesis of p-type ZnO using molecular beam epitaxy [26]. In this case, homoepitaxial nitrogen-doped ZnO was grown on semi-insulating Li-doped ZnO crystals from a high purity Zn evaporation source, combined with atomic O and N flux created via a RF plasma. Hall measurements yielded p-type behavior with a hole mobility of 2 cm^2/V s and a hole concentration of $9 \times 10^{16}/cm^3$. The acceptor level was estimated to be 170–200 meV using low temperature photoluminescence. Clearly, achieving this result was dependent on minimizing compensating donor levels from defects or complex formation.

2.1. P-type behavior in phosphorus-doped ZnO structures

While most efforts on p-type doping of ZnO have focused on nitrogen doping, a few studies have considered other group V elements for substitutional doping on the O site. Given the mismatch in ionic radii for P (2.12 Å), As (2,22 Å), and Sb (2.45 Å) as compared to O (1.38 Å), solubility of these elements in ZnO should be limited. Nevertheless, p–n junction-like behavior has been reported between an n-type ZnO substrate and a surface layer that was heavily doped with phosphorus [27]. Activation of the P dopant was achieved via laser annealing of a zinc phosphide-coated ZnO single crystal. A related result was reported for epitaxial ZnO films on GaAs subjected to annealing [28]. In this case, a p-type layer was reportedly produced at the GaAs/ZnO interface. Both of these reports are promising, but present several unresolved issues related to the solid solubility of the dopant and possible secondary phase formation in the doped region. Note that p-type doping in other II–VI compound semiconductors, using dopants with highly mismatched radii, has been reported. In particular, a shallow acceptor level is realized in ZnSe doped with nitrogen, despite the large difference in radii between Se (1.98 Å) and N (1.46 Å).

In this study, the characteristics of metal–insulator–semiconductor (MIS) and junction thin-film device structures utilizing phosphorus-doped ZnO materials are examined to delineate the carrier type in this material. Pulsed laser deposition was used for film growth. Phosphorus-doped

	GaN	ZnO
Bandgap (eV)	3.44	3.2
μ_e (cm^2/V-sec)	220	200
μ_h (cm^2/V-sec)	10	5-50
m_e	$0.27m_o$	$0.24m_o$
m_h	$0.8m_o$	$0.59m_o$
exciton binding energy (meV)	28	60

Fig. 2. Comparison of ZnO properties with those for GaN.

$(Zn_{0.9}Mg_{0.1})O$ targets were fabricated using high-purity ZnO (99.9995%) and MgO (99.998%), with P_2O_5 (99.998%) serving as the doping agent. Similar studies on P-doped ZnO films will be reported elsewhere. The motivation for considering the (Zn,Mg)O alloy resides in the potential to reduce the residual n-type conductivity due to shallow defect donor states. The addition of Mg moves the conduction band edge up in energy and potentially away from the intrinsic shallow donor state, thus increasing the activation energy of the defect donors. The ablation targets were pressed and sintered at 1000 °C for 12 h in air. Targets were fabricated with a phosphorus doping level of 2 at.%. A KrF excimer laser was used as the ablation source. A laser repetition rate of 1 Hz was used, with a target to substrate distance of 4 cm and a laser pulse energy density of 1–3 J/cm^2. The ZnO growth chamber exhibits a base pressure of 10^{-6} Torr. Platinum-coated Si was used as the substrate, with Pt serving as the bottom electrode in the device structures. Although Pt is known to form a Schottky contact with n-type ZnO, its behavior in contact with P-doped (Zn,Mg)O is unknown. However, assuming p-type conduction in the P-doped (Zn,Mg)O material, the work function of Pt makes a viable candidate as an ohmic contact. This geometry also minimizes the series resistance of the bottom contact, thus permitting a reasonably accurate measurement of the device properties. The substrates were attached to the heater platen using Ag paint. The P-doped (Zn,Mg)O layer thickness was on the order of 130 nm. The Mg, Zn, and P composition were measured using energy dispersive spectrometry and determined to be close to that of the ablation targets.

Film growth was performed at 400 °C in an oxygen pressure of 20 mTorr. Previous work has shown that as-deposited phosphorus-doped ZnO films are heavily n-type due to an apparent compensating donor defect. However, a moderate temperature anneal was shown to suppress that n-type behavior considerably. The samples were annealed in situ at a temperature of 500 °C to 600 °C in a 100 Torr O_2 ambient for 60 min. For the MIS diode structures, the P-doped (Zn,Mg)O annealing step is followed by the deposition of a gate oxide. In this case, the gate oxide selected was $(Ce,Tb)MgAl_{11}O_{19}$, which is a wide band gap insulator that can be deposited as an amorphous dielectric using pulsed laser deposition. Details of the gate dielectric properties of $(Ce,Tb)MgAl_{11}O_{19}$ will be reported elsewhere. For the p–n junction devices, an undoped ZnO film was deposited on the P-doped (Zn,Mg)O film at a temperature of 400 °C in an oxygen ambient of 20 mTorr. Previous studies have shown that this condition yields n-type ZnO with a carrier density on the order of 10^{18}–10^{19}/cm^3. The top metallization contacts for both the p–n junction and MIS device structures were 0.2 mm diameter Al or In dots that were deposited by sputter deposition through a shadow mask.

In order to delineate the carrier type in the (Zn,Mg)O:P film, capacitance–voltage characteristics of the metal–insulator–semiconductor diode structures were measured, in which the (Zn,Mg)O:P film served as the semiconductor. Capacitance–voltage behavior for Schottky barrier or metal–insulator–semiconductor diodes provide an indirect means of determining the majority carrier type in a semiconductor material. First, the symmetry of the capacitance–voltage behavior in MIS diodes is directly dependent on the carrier type underneath the gate. The total capacitance of the MIS diodes consist of two capacitances in series, one due to the insulator, a second due to the width of the depletion region underneath the gate dielectric. Depending on the majority carrier type, the MIS capacitance is maximized when the capacitor is biased such that the majority carriers accumulate at the semiconductor/insulator interface. For n-type material, a positive voltage relative to the semiconductor will attract majority carrier electrons to the interface, reduce the depletion width to near zero, and maximize capacitance. For p-type, a negative voltage is needed to accumulate majority carrier holes. In order to carefully delineate the carrier type behavior, MIS structures were fabricated with both n-type ZnO and phosphorus-doped (Zn,Mg)O thin films. Fig. 3 shows the capacitance–voltage characteristics of a structure using undoped n-type ZnO as the semiconductor. In this case, a heavily doped n-type indium–tin–oxide layer served as the bottom electrode. The polarity of the capacitance–voltage characteristic for the device employing nominally undoped ZnO is clearly n-type, with capacitance decreasing with an applied negative voltage. For a MIS diode, the net ionized dopant density, $N_A - N_D$, can be estimated from

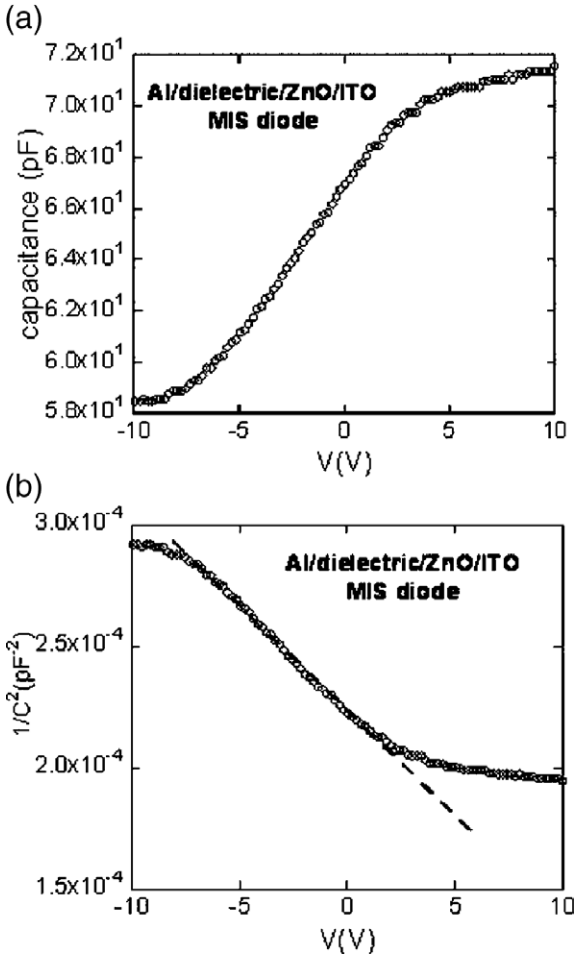

Fig. 3. Capacitance–voltage characteristics of n-type ZnO MIS diode. Plots of (a) C and (b) $1/C^2$ are included.

the capacitance–voltage behavior, where N_A is the ionized acceptor density and N_D is the donor density. In particular, for a uniformly doped semiconductor, the high frequency capacitance/area in the depletion region is given by

$$N_A - N_D = \frac{2}{q\varepsilon_s}\left[\frac{d}{dV}\left(1/C^2\right)\right]^{-1}$$

where q is the electron charge and ε_s is the permittivity of the semiconductor. Fig. 3b shows a plot of $1/C^2$ as a function of V for the diode employing n-type ZnO. From the slope, the ionized donor density is estimated to be $1.8\times10^{19}/\mathrm{cm}^3$, which is in agreement with Hall measurements for similar polycrystalline ZnO films.

Similar device structures were then fabricated that employed phosphorus-doped (Zn,Mg)O as the semiconductor material. Fig. 4 shows the capacitance–voltage behavior for these devices. The symmetry of the $C-V$ curve indicates that the (Zn,Mg)O:P film is p-type. The observation of p-type symmetry in the $C-V$ measurements was reproduced in multiple samples. Fig. 4b shows a plot of $1/C^2$ for this device. From the slope, the net acceptor concentration is calculated to be on the order of $2\times10^{18}/\mathrm{cm}^3$. If one assumes that all of the phosphorus dopant atoms are substitutional on an oxygen site,

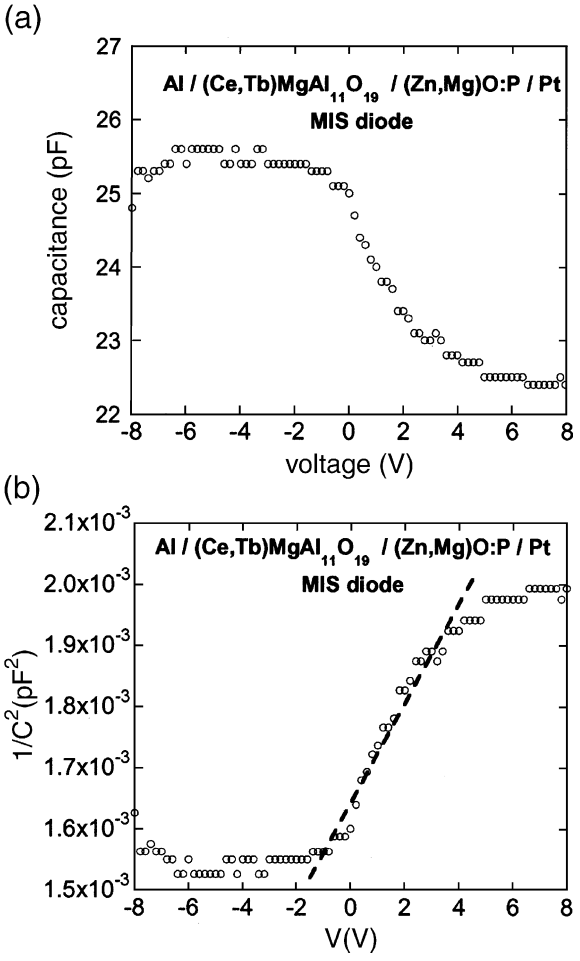

Fig. 4. Capacitance–voltage characteristics of P-doped (Zn,Mg)O MIS diode. Plots of (a) C and (b) $1/C^2$ are included.

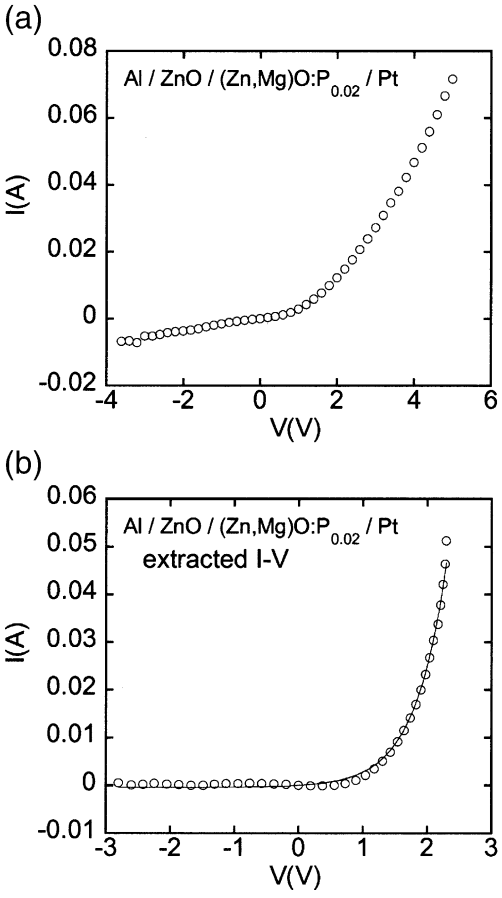

Fig. 5. $I-V$ curves for n-ZnO/P-doped (Zn,Mg)O junction. Both the raw $I-V$ (a) and extracted $I-V$ (b) are given. The solid line in (b) is a fit to the diode equation with an ideality factor greater than 10. The latter assumes a parasitic leakage conductance and series resistance.

one can estimate the activation energy based on a simple hydrogenic model. With this, the activation energy is estimated to be 250–300 meV. In addition, given that the resistivity of similar thin film material is on the order of 100–1000 Ω cm, one can estimate the magnitude of the hole mobility to be on the order of 0.01 to 0.001 $\mathrm{cm}^2/\mathrm{V\,s}$. This should not be taken as an intrinsic value of hole mobility for P-doped (Zn,Mg)O, given that the films are polycrystalline with little optimization with respect to transport properties. Nevertheless, this does explain why Hall measurements of carrier type are difficult in many samples.

In order to further delineate the carrier dynamics in P-doped (Zn,Mg)O thin films, n-ZnO/P-doped (Zn,Mg)O structures were fabricated to investigate whether p–n junction characteristics could be observed. The $I-V$ measurements were performed at room temperature. Fig. 5 shows the $I-V$ curves for a Pt/$(Zn_{0.9}Mg_{0.1})$O:$P_{0.02}$/n-ZnO/In junction. The $I-V$ curve is clearly asymmetric, with a forward bias turn-on voltage on the order of 1 V. The reverse bias breakdown voltage is on the order of 4.5 V for this particular device. Similar characteristics were also observed for other devices fabricated with Al as the top contact. The $I-V$ curves for reverse bias and strongly forward bias are nearly linear functions, suggesting the presence of a series resistance and reverse bias leakage

conductance that should be taken into account when modeling the junction transport measurements. Extracting estimates for these parasitic elements from the high forward and reverse biased conditions, a junction $I-V$ curve is extracted and shown in Fig. 5b. A reasonable fit to a p–n junction diode equation, namely $I=I_o[\exp(qV/nkT)-1]$, is then achieved and shown as the solid line. However, the ideality factor, n, extracted from the junction equation is unphysically high, estimated to be between 10 and 20 for multiple devices that were measured. High ideality factors have been observed in other non-ideal wide band gap p–n junctions, and have been attributed to space-charge limited conduction, deep-level-assisted tunneling, or parasitic rectifying junctions within the device. Nevertheless, the $I-V$ characteristics are similar to those observed for other oxide p–n heterojunctions reported elsewhere, and strongly suggests that the low carrier density, low mobility (Zn,Mg)O:P films are p-type. Attempts to observe band edge emission from the junction bias in the forward direction were unsuccessful. However, given that the carrier mobility in the (Zn,Mg)O:P layer was low, efficient light-emitting diode operation was not expected.

3. Doping for magnetism in ZnO

The field of spintronics has attracted significant attention, most recently for its potential in providing new functionality and enhanced performance in semiconducting devices, including spin-based field effect transistors (FETs), spin-polarized lasers and light-emitting diodes (LEDs), non-volatile magnetic semiconductor memory, and perhaps quantum computing [29,30]. Contemporary interest in dilute magnetic semiconductors (DMS) [31–35] has been stimulated by the discovery of ferromagnetism in Mn-doped GaAs with a T_c of 110 K [36]. This value of Curie temperature is significantly higher than that observed in previously studied DMS materials. Nevertheless, the advancement of spintronics as a technology depends upon the development and understanding of semiconductors that can support spin-polarized carrier operation at or above room temperature.

Research efforts have identified several magnetically doped semiconductors that show evidence of ferromagnetic ordering above room temperature [37–40], including transition metal-doped ZnO. As a direct wide band gap material, ZnO is of interest for photonic, electronic and magnetic applications [41,42]. Dietl et al. used Zener's model for ferromagnetism, driven by exchange interaction between hole charge carriers and localized spins, to predict ferromagnetism in p-type Mn-doped ZnO [43]. Motivated by this prediction, numerous studies have addressed the magnetic properties of transition metal-doped ZnO with conflicting conclusions regarding magnetic behavior [44–60]. In particular, for Mn-doped ZnO, Jung et al. [49] reported low T_c (45 K) ferromagnetism, whereas Fukumura et al. [50] observed spin-glass behavior with a spin-freezing temperature of 13 K. For Mn doping, we have reported ferromagnetism with a Curie temperature approaching 250 K in Mn implanted, Sn-doped bulk ZnO crystals [51]. High temperature ferromagnetism was also reported in (Zn,Mn)O by Sharma et al., with a T_c above 425 K in bulk crystals and above 300 K in thin films [40]. With an apparent T_c above 300 K, Mn-doped ZnO is attractive for spintronic technology. Moreover, this material is useful in delineating the origin of ferromagnetism in a semiconductor host, primarily due to a lack of ferromagnetic secondary phases in the Zn–Mn–O phase diagram. For other transition metal dopants, the possible presence of secondary ferromagnetic phases can not be easily eliminated as the origin of the magnetic signals. For Mn-doped ZnO, the only ferromagnetic composition for this solid solution is Mn_3O_4, which is ferrimagnetic with a Curie temperature less than 50 K [61,62]. Therefore, any room temperature ferromagnetism cannot be assigned to known secondary phases as none exist.

While experiments indicate high-temperature ferromagnetism in these materials, there remain some questions regarding the origin of the magnetic behavior in Mn-doped ZnO materials. Dietl's work predicted that highly p-type, Mn-doped ZnO should have Curie temperatures in excess of room temperature [43,63,64]. The theory assumes that ferromagnetic ordering between the localized moments of the Mn atoms is mediated by free holes in the material. While high hole concentrations are predicted to yield high Curie temperatures, carrier-mediated ferromagnetism in n-type material should be limited to lower temperatures. This distinction in carrier type is attributed to the smaller density of states and exchange integral for Mn with the conduction band in comparison to the valence band [65], as the Mn^{2+} state lies within the valence band of these materials. It is important to recognize that the exchange interaction for Mn, when placed in the wide band gap semiconductors, is fundamentally different from the other transition metal ions. Mn d-states lie in the valence band while the other transition metals d-state orbitals introduce states within the gap. There are apparent discrepancies between Dietl's model and the experimental results for Mn-doped ZnO. In these materials, ferromagnetism has been reported in n-type and/or semi-insulating samples. In fact, achieving high hole carrier density in ZnO is a significant challenge that is being actively pursued for electronic applications [66]. An alternative model addresses whether ferromagnetic ordering of the Mn moments could originate from carriers (holes) that are present in the material, but localized at the transition metal impurity [67,68]. The bound magnetic polaron model assumes an exchange interaction between the transition metal (Mn) ion and localized (trapped) holes that are spatially near the Mn ion. As temperature decreases, the size of the bound magnetic polaron grows until its radius overlaps that of neighboring polarons. This enables ferromagnetic ordering of the Mn ions in an otherwise insulating or semi-insulating material. Predictions based on this bound magnetic polaron model suggest that ferromagnetic ordering is possible. However, for Mn, it still depends on the availability of holes, albeit a localized distribution.

4. Experiments for Mn,Sn-doped ZnO

Epitaxial Mn,Sn-doped ZnO films were grown by conventional pulsed laser deposition. Laser ablation targets were

prepared from high purity powders of ZnO (99.999%), with MnO_2 (99.999%) and SnO_2 (99.95%) serving as the doping agents. The pressed targets were sintered at 1000 °C for 12 h in air. The targets were fabricated with a nominal composition of 3 at.% Mn and 0, 0.1, 0.01, and 0.001 at.% Sn. A Lambda Physik KrF excimer laser was used as the ablation source. The laser energy density was 1–3 J/cm^2 with a laser repetition rate of 1 Hz and target-to-substrate distance of 6 cm. The growth chamber exhibits a base pressure of 10^{-5} Torr. Films were deposited onto single crystal, *c*-plane oriented sapphire substrates. Film growth was conducted over a temperature range of 400–600 °C. An oxygen pressure of 20 mTorr was used for all film growth experiments. Film thicknesses were approximately 300 to 400 nm. X-ray diffraction was used to determine the crystallinity and secondary phase formation. SQUID magnetometry was used to characterize the ferromagnetic behavior of the doped films, focusing on the films grown at 400 °C.

5. Results for Mn,Sn-doped ZnO

The phase stability and solid solubility of Mn in the ZnO films were investigated as a function of growth temperature for films with varying Sn concentrations. Fig. 6 shows the X-ray diffraction scans for films deposited under the given growth conditions. In all cases, the dominant film peaks correspond to c-axis perpendicular ZnO. Note that, for some of the films, segregation of the Mn_3O_4 phase is evident in the diffraction data. As mentioned earlier, the Mn_3O_4 phase is ferromagnetic with a Curie temperature less than 50 K. The narrow peak located near 31° is an artifact peak from the sapphire substrate. Previous reports from Fukumura et al. indicated that epitaxial ZnO films with a Mn concentration as high as 35% could be achieved while maintaining the wurtzite structure using pulsed laser deposition [69]. In this study, we find evidence for Mn oxide precipitation at a Mn concentration of only 3 at.% Mn, although the intensity of diffraction peaks from Mn_3O_4 varies with growth temperatures and Sn concentrations. This discrepancy between this work and

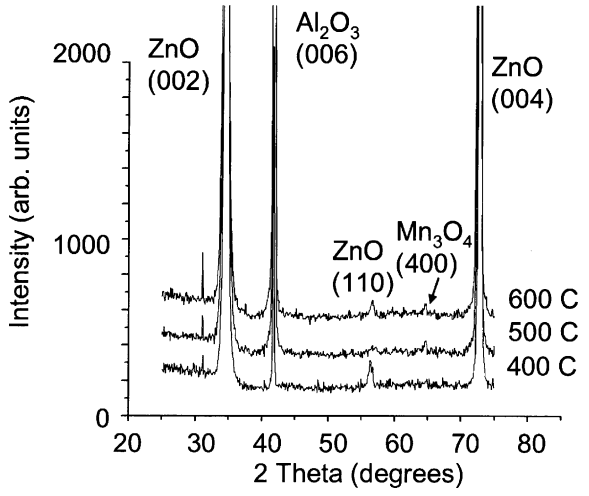

Fig. 6. X-ray diffraction of ZnO films co-doped with Mn and Sn grown at an oxygen partial pressure of 20 mTorr and growth temperatures of 400, 500, and 600 °C. The target was ZnO doped with 3% Mn and 0.01% Sn.

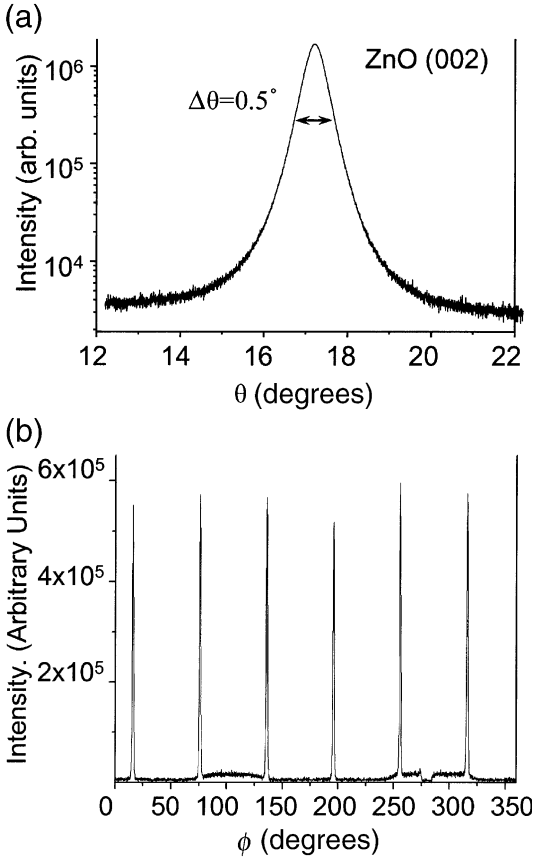

Fig. 7. X-ray diffraction of an epitaxial ZnO film doped with 3% Mn and 0.1% Sn that was deposited at 500 °C and $p(O_2)$=20 mTorr: (a) an ω-rocking curve of the ZnO (002) peak with a FWHM of 0.5°; (b) in-plane ϕ scan of the ZnO (101) planes.

that of Fukumura might be attributed to the higher oxygen pressure used in our experiments (20 mTorr) as compared to 5×10^{-5} Torr in Fukumura's experiments. Note that the precipitation of Sn-containing phases is not observed in the diffraction scan, nor is it expected even if present as the nominal concentration of Sn in the films is $\leq$0.1%.

The epitaxial nature of the ZnO films was determined using four-circle high-resolution X-ray diffraction. Fig. 7a shows the X-ray diffraction ω-scan about the ZnO (002) peak for the film grown on *c*-plane sapphire substrate at a growth temperature of 500 °C and Sn concentration of 0.1%. The ZnO (002) rocking curve displays a full-width at half maximum (FWHM) of 0.5°. The in-plane alignment is evident in the ϕ-scan of the ZnO (101) plane shown in Fig. 7b. The ϕ-scan peaks at 60° intervals are consistent with the hexagonal symmetry of the epitaxial ZnO wurtzite structure.

The room temperature resistivity for Mn-doped ZnO films with varying concentrations of Sn was determined using a four-point van der Pauw geometry. Defect chemistry calculations for Mn-doped ZnO indicate that Mn^{2+} forms a donor level ~2.0 eV below the conduction band edge [70]. This deep donor state with Mn substitution on the Zn site in ZnO has no direct effect on the electron concentration at room temperature. However, defect chemistry calculations also indicate a reduction in Zn interstitials with Mn doping. Zn interstitials are generally

Table 1
Resistivity as a function of Sn content in co-doped ZnO:3% Mn films

	Sn concentration (%)			
	0.0	0.001	0.01	0.1
Resistivity (Ω cm)	195	320	17	0.185

accepted as the primary shallow donor defects in nominally undoped ZnO. This will yield an increase in resistivity for Mn-doped films as compared to undoped material [70–72]. The Mn-doped ZnO films with no Sn exhibit a resistivity on the order of 10^2 Ω cm with a carrier density of mid-10^{16}/cm^3. This carrier density is substantially lower than that seen for undoped epitaxial films, and is consistent with the reduction of shallow donors. Limited results on the doping behavior of Sn in ZnO indicate that it introduces a donor state [73–77], although in some II–VI compound semiconductors, Sn is an amphoteric dopant, substituting on either the II or VI site [78,79]. For ZnO, the expectation is that Sn will substitute on the Zn site due to a close match in ionic radii between Zn^{2+} (0.074 nm) and Sn^{4+} (0.069 nm). For the epitaxial films considered in this work, Sn behaves as a donor. The resistivity of ZnO:Mn films with various Sn content is shown in Table 1. The resistivity of the films drops rapidly with Sn doping, with a minimum of 0.185 Ω cm for a Sn concentration of 0.1%. The most common valence state of Sn is +4, yielding a doubly ionized donor if doped substitutionally on the Zn site. Hall measurements indicate that the films are increasingly n-type with Sn doping up to 0.1 at.%. It should also be noted that other work has shown that the addition of Sn to ZnO ceramics also yields an enhancement in crystallinity [73,74].

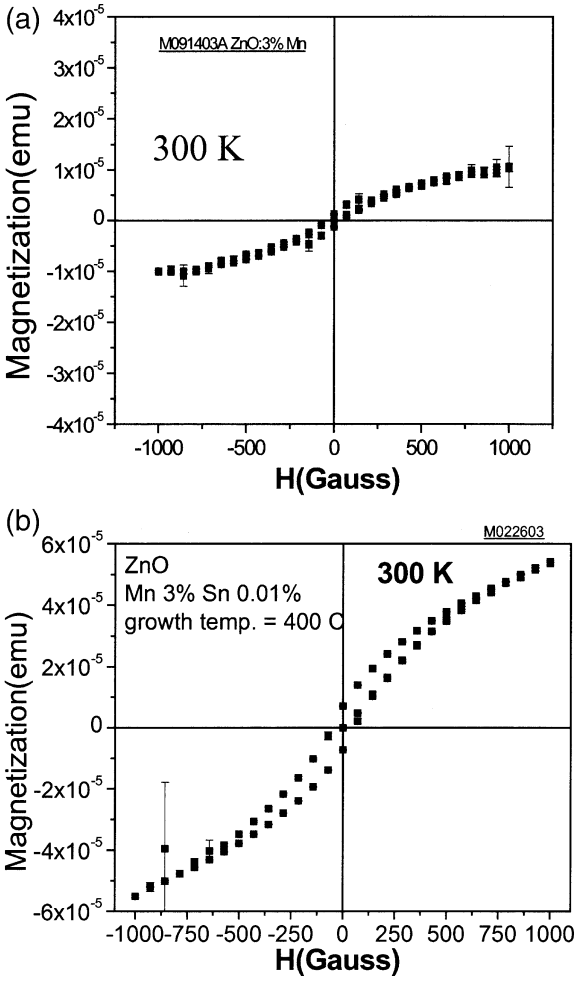

Fig. 8. SQUID measurements for epitaxial ZnO:3% Mn films without (a) and with (b) Sn co-doping. Notice that the film without Sn exhibits little or no hysteresis, whereas the film with Sn shows hysteresis.

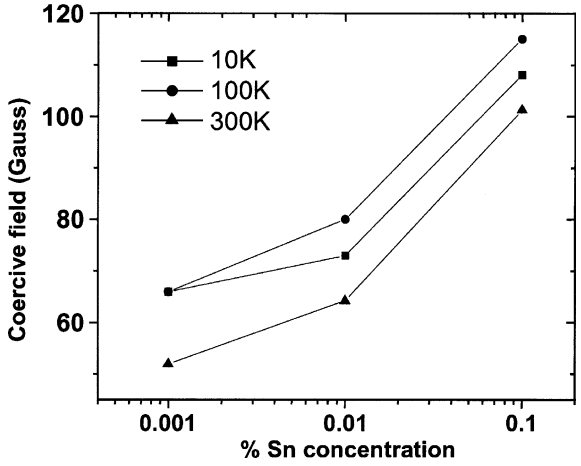

Fig. 9. A plot showing the dependence of the coercive field on Sn concentration at different SQUID measurement temperatures.

The magnetic properties of the films were measured using a Quantum Design SQUID magnetometer. The diamagnetic responses of the substrate and host semiconductor were subtracted from the magnetization plots. The primary focus of the measurements was to determine how the magnetic properties of the films changed as a function of electron density as controlled by Sn concentration. Samples that showed minimal amounts of Mn_3O_4 precipitation via X-ray diffraction were used for the SQUID measurements. Fig. 8 shows the magnetization as a function of applied magnetic field for epitaxial ZnO:3% Mn films both without (a) and with (b) Sn co-doping. For the Mn-doped film with no Sn, saturation in the magnetization is observed, but with little evidence for hysteresis in the M vs. H curves. In contrast, the ZnO film doped with both Mn and Sn exhibits clear hysteresis. From the

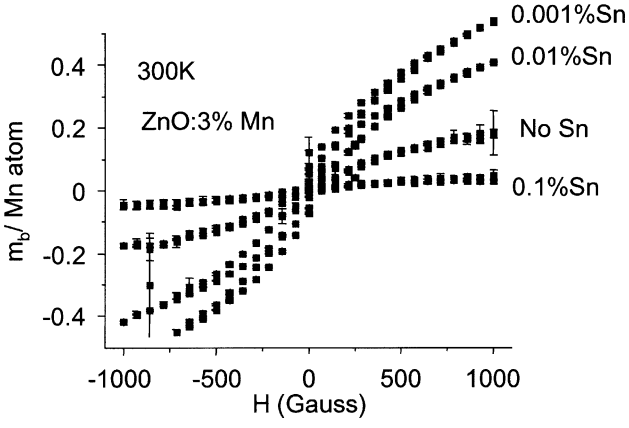

Fig. 10. Magnetization measured at 300 K for epitaxial ZnO:3% Mn films that are co-doped with 0.001% Sn, 0.01% Sn, 0.1% Sn, and no Sn. There appears to be an inverse correlation of the Sn content with the saturation magnetization.

hysteresis curves, one can also observe an increase in loop width with increasing Sn concentration. Fig. 9 shows the coercive field as a function of Sn concentration, suggesting domain pinning as the Sn doping is increased. It is unclear why the addition of Sn enhances the hysteretic magnetization response in Mn-doped films. It might indicate enhanced pinning of domains due to the Sn dopants.

Most interesting is the saturation magnetization behavior as Sn content is increased. As noted earlier, increasing Sn concentration increases electron density and conductivity. Fig. 10 shows the room temperature magnetization versus field behavior for the ZnO samples containing 3% Mn and Sn contents of 0, 0.1, 0.01, and 0.001%. Magnetization is given as the magnetic moment/Mn dopant ion. Initially, there is an increase in magnetization with minimal Sn doping. However, with increasing Sn doping, there is an inverse correlation between the Sn content and saturation magnetization. As the electron density increases with Sn doping, the magnetization decreases. The maximum magnetization corresponds to a magnetic moment/Mn ion of ~0.5 Bohr magnetrons/Mn. This is consistent with the bound magnetic polaron model in which only a fraction of the Mn ions are expected to order ferromagnetically due to competing superexchange antiferromagnetic interactions between neighboring Mn ions [80]. The inverse correlation of saturation magnetization with electron density is interesting and provides some insight into the mechanism for ferromagnetism in Mn-doped ZnO. This has been observed via P-doped in Mn-doped ZnO films as well. Overlap of the Mn d-states with the valence band suggests that holes are necessary in order to induce ferromagnetic order. For semi-insulating films to exhibit ferromagnetism, the bound magnetic polaron model provides a mechanism whereby holes that are localized at or near the Mn ions are responsible for mediating ferromagnetism. The addition of electrons to the system will move the Fermi energy level up in the band gap, resulting in a decrease in hole density and a reduction in magnetization. This appears consistent with early work on trivalent doped (Zn,Mn)O where no ferromagnetism was observed for heavily n-type films. It may also explain the discrepancy from other studies of Mn-doped ZnO films in which the intrinsic defect-mediated donor states are high in density. It is important to note the need to maintain a Mn concentration low enough to avoid Mn–Mn antiferromagnetic interactions, which are likely to dominate high Mn-doped ZnO films.

Acknowledgments

This work was supported by the Army Research Laboratory, the Air Force Office of Scientific Research, and the National Science Foundation.

References

[1] A.R. Hutson, Phys. Rev. 108 (1957) 222.
[2] D.C. Look, J.W. Hemsky, J.R. Sizelove, Phys. Rev. Lett. 82 (1999) 2552.
[3] B.J. Jin, S.H. Bae, S.Y. Lee, S. Im, Mater. Sci. Eng., B 71 (2000) 301.
[4] D.M. Hofmann, A. Hofstaetter, F. Leiter, Hhuijuan Zhou, F. Henecker, B.K. Meyer, S.B. Orlinskii, J. Schmidt, P.G. Baranov, Phys. Rev. Lett. 88 (2002) 045504.
[5] C.G. Van de Walle, Phys. Status Solidi, B 229 (2002) 221.
[6] S.F.J. Cox, E.A. Davis, P.J.C. King, J.M. Gil, H.V. Alberto, R.C. Vilao, J. Piroto Duarte, N.A. De Campos, R.L. Lichti, J. Phys.: Condens. Matter 13 (2001) 9001.
[7] C.G. Van de Walle, Phys. Rev. Lett. 85 (2000) 1012.
[8] L.K. Singh, H. Mohan, Indian J. Pure Appl. Phys. 13 (1975) 486.
[9] C.W. Teng, J.F. Muth, U. Ozgur, M.J. Bergmann, H.O. Everitt, A.K. Sharma, C. Jin, J. Narayan, Appl. Phys. Lett. 76 (2000) 979.
[10] A. Ohtomo, M. Kawasaki, Y. Sakurai, I. Ohkubo, R. Shiroki, Y. Yoshida, T. Yasuda, Y. Segawa, H. Koinuma, Mater. Sci. Eng., B 56 (1998) 263.
[11] T. Makino, K. Tamura, C.H. Chia, Y. Segawa, M. Kawasaki, A. Ohtomo, H. Koinuma, Appl. Phys. Lett. 81 (2002) 2172.
[12] G.F. Neumark, in: H.E. Ruda (Ed.), Widegap II–VI Compounds for Opto-Electronics Applications, 1992, p. 281.
[13] D.B. Laks, C.G. Van de Walle, G.F. Neumark, S.T. Pantelides, Appl. Phys. Lett. 63 (1993) 1375.
[14] Y. Kanai, Jpn. J. Appl. Phys. Part 1 (Reg. Pap. Short Notes) 30 (1991) 703.
[15] Y. Kanai, Jpn. J. Appl. Phys. Part 1 (Reg. Pap. Short Notes) 30 (1991) 2021.
[16] J.A. Savage, E.M. Dodson, J. Mater. Sci. 4 (1969) 809.
[17] A. Valentini, F. Quaranta, M. Rossi, G. Battaglin, J. Vac. Sci. Technol., A 9 (1991) 286.
[18] C.H. Park, S.B. Zhang, Wei Su Huai, Phys. Rev. B 66 (2002) 286.
[19] T. Yamamoto, H. Katayama-Yoshida, Jpn. J. Appl. Phys. 38 (1999) L166.
[20] N.Y. Garces, N.C. Giles, L.E. Halliburton, G. Cantwell, D.B. Eason, D.C. Reynolds, D.C. Look, Appl. Phys. Lett. 80 (2002) 1334.
[21] K. Minegishi, Y. Koiwai, Y. Kikuchi, K. Yano, M. Kasuga, A. Shimizu, Jpn. J. Appl. Phys. 36 (1997) L1453.
[22] Xin-Li Guo, H. Tabata, T. Kawai, J. Cryst. Growth 223 (2001) 135.
[23] C. Rouleau, S. Kang, D. Lowndes, unpublished.
[24] K. Iwata, P. Fons, A. Yamada, K. Matsubara, S. Niki, J. Cryst. Growth 209 (2000) 526.
[25] Y. Yan, S.B. Zhang, S.T. Pantelides, Phys. Rev. Lett. 86 (2001) 5723.
[26] D.C. Look, D.C. Reynolds, C.W. Litton, R.L. Jones, D.B. Eason, G. Cantwell, Appl. Phys. Lett. 81 (2002) 1830.
[27] T. Aoki, Y. Hatanaka, D.C. Look, Appl. Phys. Lett. 76 (2000) 3257.
[28] Y.R. Ryu, S. Zhu, D.C. Look, J.M. Wrobel, H.M. Jeong, H.W. White, J. Cryst. Growth 216 (2000) 330.
[29] S.A. Wolf, D.D. Awschalom, R.A. Buhrman, J.M. Daughton, S. von Molnár, M.L. Roukes, A.Y. Chtchelkanova, D.M. Treger, Science 294 (2001) 1488.
[30] G.A. Prinz, Science 282 (1998) 1660.
[31] J.K. Furdyna, J. Appl. Phys. 64 (1988) R29.
[32] S. Gopalan, M.G. Cottam, Phys. Rev. B 42 (1990) 10311.
[33] C. Haas, Crit. Rev. Solid State Sci. 1 (1970) 47.
[34] T. Suski, J. Igalson, T. Story, J. Magn. Magn. Mater. 66 (1987) 325.
[35] A. Haury, A. Wasiela, A. Arnoult, J. Cibert, S. Tatarenko, T. Dietl, Y. Merle d'Aubigne, Phys. Rev. Lett. 79 (1997) 511.
[36] H. Ohno, Science 281 (1998) 951.
[37] S.J. Pearton, C.R. Abernathy, D.P. Norton, A.F. Hebard, Y.D. Park, L.A. Boatner, J.D. Budai, Mater. Sci. Eng., R 40 (2003) 137.
[38] M. Ivill, M.E. Overberg, C.R. Abernathy, D.P. Norton, A.F. Hebard, N. Theodoropoulou, J.D. Budai, Solid-State Electron. 47 (2003) 2215.
[39] Yuji Matsumoto, Makoto Murakami, Tomoji Shono, Tetsuya Hasegawa, Tomotero Fukumura, Masashi Kawasaki, Parhat Ahmet, Toyohiro Chikyow, Shin-ya Koshihara, Hideomi Koinuma, Science 291 (2001) 854.
[40] P. Sharma, A. Gupta, K.V. Rao, F.J. Owens, R. Sharma, R. Ahuja, J.M. Osorio Guillen, B. Johansson, G.A. Gehring, Nat. Mater. 2 (2003) 673.
[41] D.C. Look, Mater. Sci. Eng., B 80 (2001) 383.
[42] Satoshi Masuda, Ken Kitamura, Yoshihiro Okumura, Shigehiro Miyatake, Hitoshi Tabata, Tomoji Kawai, J. Appl. Phys. 93 (2003) 1624.
[43] T. Dietl, H. Ohno, F. Matsukura, J. Cubert, D. Ferrand, Science 287 (2000) 1019.
[44] K. Sato, H. Katayama-Yoshida, Jpn. J. Appl. Phys. 39 (2000) L555.

[45] Jae Hyun Kim, Hyojin Kim, Dojin Kim, Young Eon Ihm, Woong Kil Choo, J. Appl. Phys. 92 (2002) 6066.
[46] Hyeon-Jun Lee, Se-Young Jeong, Chae Ryong Cho, Chul Hong Park, Appl. Phys. Lett. 81 (2002) 4020.
[47] T. Wakano, N. Fujimura, Y. Morinaga, N. Abe, A. Ashida, T. Ito, Physica E 10 (2001) 260.
[48] S.-J. Han, J.W. Song, C.-H. Yang, S.H. Park, J.-H. Park, Y.H. Jeong, K.W. Rhie, Appl. Phys. Lett. 81 (2002) 4212.
[49] S.W. Jung, S.-J. An, G.-C. Yi, C.U. Jung, S.-I. Lee, S. Cho, Appl. Phys. Lett. 80 (2002) 4561.
[50] T. Fukumura, M. Zhengwu Jin, T. Kawasaki, T. Shono, S. Hasegawa, H. Koshihara, Appl. Phys. Lett. 78 (2001) 958.
[51] D.P. Norton, S.J. Pearton, Hebard N. Theodoropoulou, L.A. Boatner, R.G. Wilson, Appl. Phys. Lett. 82 (2003) 239.
[52] M.S. Park, B.I. Min, Phys. Rev. B 68 (2003) 224436.
[53] Y.Q. Chang, D.B. Wang, X.H. Luo, X.Y. Xu, X.H. Chen, L. Li, C.P. Chen, R.M. Wang, J. Xu, D.P. Yu, Appl. Phys. Lett. 83 (2003) 4020.
[54] A.S. Risbud, N.A. Spaldin, Z.Q. Chen, S. Stemmer, R. Seshadri, Phys. Rev. B 68 (2003) 205202.
[55] S.-J. Han, T.–H. Jang, Y.B. Kim, B.–G. Park, J.-H. Park, Y.H. Jeong, Appl. Phys. Lett. 83 (2003) 920.
[56] S.W. Yoon, S.-B. Cho, S.C. We, S. Yoon, B.J. Suh, H.K. Song, Y.J. Shin, J. Appl. Phys. 93 (2003) 7879.
[57] V.A.L. Roy, A.B. Djurisic, H. Liu, X.X. Zhang, Y.H. Leung, M.H. Xie, J. Gao, H.F. Lui, C. Surya, Appl. Phys. Lett. 84 (2004) 756.
[58] X.M. Cheng, C.L. Chien, J. Appl. Phys. 93 (2003) 7876.
[59] S.S. Kim, J.H. Moon, B.-T. Lee, O.S. Song, J.H. Je, J. Appl. Phys. 95 (2004) 454.
[60] S. Kolesnik, B. Dabrowski, J. Mais, J. Appl. Phys. 95 (2004) 2582.
[61] L.W. Guo, D.L. Peng, H. Makino, K. Inaba, H.J. Ko, K. Sumiyama, Y. Yao, J. Magn. Magn. Mater. 213 (2000) 321.
[62] A. Chartier, P. D'Arco, R. Dovesi, V.R. Saunders, Phys. Rev. B 60 (1999) 14042.
[63] T. Dietl, A. Haury, Y. Merle d'Aubigne, Phys. Rev. B 55 (1997) R3347.
[64] T. Dietl, Semicond. Sci. Technol. 17 (2002) 377.
[65] H. Ohno, in: D.D. Awschalom, D. Loss, N. Samarth (Eds.), Chpt. 1 in Semiconductor Spintronics and Quantum Computation, Springer, 2002.
[66] D.C. Look, D.C. Reynolds, C.W. Litton, R.L. Jones, D.B. Eason, G. Cantwell, Appl. Phys. Lett. 81 (2002) 1830.
[67] A. Kaminski, S. Das Sarma, Phys. Rev. Lett. 88 (2002) 247202-1.
[68] M. Berciu, R.N. Bhatt, Phys. Rev. Lett. 87 (2001) 107203.
[69] T. Fukumura, Z. Jin, A. Ohtomo, H. Koinuma, M. Kawasaki, Appl. Phys. Lett. 75 (1999) 3366.
[70] J. Han, P.Q. Mantas, A.M.R. Senos, J. Eur. Ceram. Soc. 22 (2002) 49.
[71] Z. Zhou, K. Kato, T. Komaki, M. Yoshino, H. Yukawa, M. Morinaga, K. Morita, J. Eur. Ceram. Soc. 24 (2004) 139.
[72] N. Ohashi, J. Tanaka, T. Ohgaki, H. Haneda, M. Ozawa, T. Tsurumi, J. Mater. Res. 17 (2002) 1529.
[73] F. Paraguay, J. Morales, W. Estrada, E. Andrade, M. Miki-Yoshida, Thin Solid Films 366 (2000) 16.
[74] A. Bougrine, A. El. Hichou, M. Addou, J. Ebothé, A. Kachouane, M. Troyon, Mater. Chem. Phys. 80 (2003) 438.
[75] J.-H. Lee, B.-O. Park, Thin Solid Films 426 (2003) 94.
[76] H. Sato, T. Minami, S. Takata, J. Vac. Sci. Technol., A 11 (1993) 2975.
[77] E. Holmelund, J. Schou, S. Tougaard, N.B. Larsen, Appl. Surf. Sci. 197 (2002) 467.
[78] I. Turkevych, R. Grill, J. Franc, P. Höschl, E. Belas, P. Moravec, Cryst. Res. Technol. 38 (2003) 288.
[79] O. Panchuk, A. Savitskiy, P. Fochuk, Y. Nykonyuk, O. Parfenyuk, L. Shcherbak, M. Ilashchuk, L. Yatsunyk, P. Feychuk, J. Cryst. Growth 197 (1999) 607.
[80] T. Dietl, M. Sawicki, L. Van Khoi, J. Jaroszyñski, P. Kossacki, J. Cibert, D. Ferrand, S. Tatarenko, A. Wasiela, Phys. Status Solidi, B 229 (2002) 665.